Available online at www.sciencedirect.com
SCIENCE DIRECT®
Journal of Solid State Chemistry 177 (2004) 3092–3098
JOURNAL OF SOLID STATE CHEMISTRY
http://elsevier.com/locate/jssc

Hydroxyapatite gels and nanocrystals prepared through a sol–gel process

A. Bigi,* E. Boanini, and K. Rubini

Department of Chemistry "G. Ciamician", University of Bologna, via Francesco Selmi, n. 2 40126 Bologna, Italy

Received 30 March 2004; received in revised form 11 May 2004; accepted 12 May 2004

Available online 26 June 2004

Abstract

We have investigated the effect of the Ca/P molar ratio on the structural and morphological properties of hydroxyapatite (HA) gels and nanocrystals. The sol–gel process was carried out in aqueous, and alternatively in alcoholic medium (50% water–50% ethanol), at 37°C. Gel samples were obtained by drying the sols at 37°C or at 80°C, whereas powder samples were obtained by filtering the sols. Heat treatment at temperatures as low as 300°C is enough to obtain pure HA from the gels with a Ca/P molar ratio of 1.00 and 1.67. At variance, heat treatment of the gels with a Ca/P of 2.55 always produces secondary phases. The degree of crystallinity of HA increases with the Ca/P molar ratio of the sols, and it is slightly affected by the presence of ethanol in the precipitation medium. Filtering of the sols provides powders constituted of nanocrystalline HA that exhibit degree of crystallinity, crystal morphology and thermal stability closely related to the sols composition.

Keywords: Hydroxyapatite; Sol–gel; Crystallinity; Ca/P molar ratio; Nanocrystals

1. Introduction

Thanks to its chemical and structural similarity with the mineral phase of bone and teeth, synthetic hydroxyapatite, $Ca_{10}(PO_4)_6(OH)_2$ (HA), is widely used for hard tissues repair. The different clinical applications involve repair of bone defects, bone augmentation, as well coatings for metallic implants [1,2]. One of the most important requirement of a material designed for bone substitution and/or repair, is the ability to create a bond with the host living bone [3]. To this aim, a high degree of crystallinity and chemical stability have been included among the desirable properties of an ideal hydroxyapatite [4,5]. At variance, a poor degree of crystallinity associated to a greater resorbability has been shown to be more effective for promoting early bone ingrowth [6]. This is in agreement with the characteristics of biological apatites, which are typically non-crystalline and non-stoichiometric. The chemical, structural and morphological properties of synthetic HA can be modulated by varying the method and the conditions of synthesis. Classical methods for HA powder synthesis include direct precipitation, hydrothermal techniques, hydrolysis of other calcium phosphates, as well as solid-state reactions [2,7]. Among the alternative methods, sol–gel synthesis of HA ceramics has recently attracted much attention, due to its many advantages, which include high product purity, homogeneous composition, and low synthesis temperature [8]. Moreover, the sol–gel process is easily applicable to surface coating, and it allows the preparation of high-quality HA thin films on metal substrates [8–11]. Thus, the sol–gel process can be usefully utilized to synthesize both nanocrystalline HA powders and HA films under significantly mild conditions. Aging of the precursor solutions was found to be critical in developing an apatitic phase [12]. The speed of gelation, the chemistry of the precursors, and the nature of the solvent, are among the main factors affecting the process [9–11,13–15].

We have used a water based sol–gel synthesis of hydroxyapatite to investigate the effect of several parameters, such as Ca/P molar ratio, presence of ethanol in the precipitation medium, and drying

*Corresponding author. Fax: +39-051-209-9456.
E-mail address: adriana.bigi@unibo.it (A. Bigi).

0022-4596/$ - see front matter © 2004 Elsevier Inc. All rights reserved.
doi:10.1016/j.jssc.2004.05.018

temperature, on the structural and morphological properties of HA gels and powders.

2. Materials and methods

The starting materials used in the synthesis of hydroxyapatite were analytical grade reagents $Ca(NO_3)_2{\cdot}4H_2O$ and $(NH_4)_2HPO_4$. $Ca(NO_3)_2 \cdot 4H_2O$ was dissolved in 50 mL of deionized water at 37°C and rapidly added to a 50 mL solution containing $(NH_4)_2HPO_4$ at 37°C under stirring. The concentrations of the reactants were varied in order to obtain a Ca/P molar ratio in solution of 1.00, 1.67, and 2.55. Before mixing, the pH value of the solutions was adjusted above 9 with NH_4OH. The syntheses in alcoholic medium were carried out following the same procedure as for aqueous medium, but dissolving $Ca(NO_3)_2{\cdot}4H_2O$, as well as $(NH_4)_2HPO_4$, in 25 mL of deionized water and 25 mL of ethanol.

The powder products were obtained by filtering the solutions after 3 min of stirring at 37°C. The filtered products were repeatedly washed, and dried at 37°C overnight.

Gels were obtained by drying the sols after 3 min of stirring at 37°C. A part of the sol was dried at 37°C, whereas a second part was oven-dried at 80°C overnight. The conditions of preparation of the different gels are summarized in Table 1.

X-ray diffraction analysis was carried out by means of a Philips PW 1050/81 powder diffractometer equipped with a graphite monochromator in the diffracted beam. Cu$K\alpha$ radiation was used (40 mA, 40 kV). The 2θ range was from 10° to 60° at a scanning speed of 0.75°/min. In order to evaluate the coherence length of the apatitic crystals, further X-ray powder data were obtained in two regions, peak (002) between 24.5 and 27.5 of 2θ and peak (310) between 37.5 and 41.5 of 2θ by means of step scans using a fixed counting time period of 10 s and a scan rate of 0.020°/step. The silicon standard peak 1 1 1 was used to evaluate the instrumental broadening.

For IR adsorption analysis, 1 mg of the powdered samples was carefully mixed with 300 mg of KBr (infrared grade) and pelletised under a pressure of 10 tons for 2 min. The pellets were analyzed using a Nicolet FT 205 IR spectrophotometer to collect 32 scans in the range 4000–400 cm^{-1} at a resolution of 4 cm^{-1}.

Calcium and phosphorus contents were determined by means of a Dionex DX100 chromatography system equipped with a Dionex CD20 conductivity detector. Powders were previously dissolved in 0.1 M HCl. The chromatographic data were collected and processed with Dionex peaknet 5.1 program.

Thermogravimetric analysis was carried out using a Perkin Elmer TGA-7. Heating was performed in a platinum crucible in air flow (20 cm^3/min) at a rate of 5°C/min up to 900°C. The samples weights were in the range 5–10 mg.

Table 1
Conditions of preparation of the different gels

Gel	Precipitation medium	Ca/P	Drying temperature (°C)
W-100-37	Water	1.00	37
W-100-80	Water	1.00	80
A-100-37	Alcohol/water	1.00	37
A-100-80	Alcohol/water	1.00	80
W-167-37	Water	1.67	37
W-167-80	Water	1.67	80
A-167-37	Alcohol/water	1.67	37
A-167-80	Alcohol/water	1.67	80
W-255-37	Water	2.55	37
W-255-80	Water	2.55	80
A-255-37	Alcohol/water	2.55	37
A-255-80	Alcohol/water	2.55	80

Morphological investigation of the samples was performed using a Philips XL-20 scanning electron microscope operating at 20 kV. The samples were sputter-coated with gold prior to examination.

For TEM investigations, specimens were sonicated in order to split aggregates, without any additional treatment. A drop of the calcium phosphate suspension was transferred onto holey carbon foils supported on conventional copper microgrids. A Philips CM 100 transmission electron microscope operating at 80 kV was used.

3. Results and discussion

3.1. Gels characterization

Both the ethanol- and aqueous-based sols transform into solid gels upon heating at 80°C for 15 h. The transformation occurs more slowly at 37°C for the aqueous sols, and even more for the viscous ethanol-based gels, which require at least 3 days to dry. Thermogravimetric analysis shows that the dried gels display a thermal transition in the temperature region 200–300°C, which corresponds to a weight loss of about 60 wt%, as shown in the plot of the W-167-37 gel reported in Fig. 1a. The weight loss is associated with the removal of nitrate and ammonium from the gels, and it displays similar features for the different samples, even if it occurs in a range of temperature slightly wider for the 2.55 gels when the process is completed at about 350°C. The thermogravimetric plot of the A-255-37 gel reported in Fig. 1b, shows the presence of a further thermal process between 450°C and 550°C, corresponding to a weight loss of about 10 wt%. This further weight loss, which can be appreciated in the plots of all the 2.55 gels, could be due to the combustion of the

decomposition products that form in presence of excess nitrate. In agreement with their greater viscosity, the ethanol-based gels exhibit a further, small weight loss between 100°C and 200°C, indicating the evaporation of ethanol and water [8], which is probably promoted by the destructuration effect of ethanol [16].

The powder X-ray diffraction patterns of the dried gels display the most intense peaks of hydroxyapatite, together with those characteristic of ammonium nitrate, as shown by the comparison among the patterns recorded from the W-100-80, W-167-80, and W-255-80 samples reported in Figs. 2a–c. The patterns recorded from the A-gels are quite similar to those of the W-gels, and do not show any significant variation as a function of the drying temperature. The X-ray diffraction patterns obtained from the gels after heat treatment at 300°C display just the diffraction peaks of HA, suggesting the complete removal of nitrate. However, the degree of crystallinity of the apatitic phase obtained after heat treatment at 300°C of the gels prepared with a Ca/P ratio of 1.00 (Fig. 2d) appears significantly lower than that of the gels at Ca/P of 1.67 and 2.55 (Fig. 2e,f). The line broadening of the 0 0 2 and 3 1 0 reflections was used to evaluate the length of the coherent domains (τ_{hkl}) of the apatitic phases obtained after heat treatment of the gels at 300°C. $\tau_{h\,k\,l}$ values were calculated along the *c*-axis and along a direction perpendicular to it from the widths at half maximum intensity ($\beta_{1/2}$) using the Scherrer equation [17]:

$$\tau_{h\,k\,l} = \frac{k\lambda}{\beta_{1/2}\cos\theta},$$

where λ is the wavelength, θ the diffraction angle and K a constant depending on crystal habit (chosen as 0.9). The instrumental broadening was taken into account. The $\tau_{h\,k\,l}$ values increase as a function of the Ca/P molar ratio of the gels. The coherence lengths of the perfect crystalline domains increase both along the *c*-axis direction and along the orthogonal direction, as shown in the graphs reported in Figs. 3a and b. The increase along the 0 0 2 direction appears slightly greater for the A-gels than for the W-gels, whereas the precipitation medium, as well as the temperature of air drying of the sols, do not affect significantly the $\tau_{3\,1\,0}$ values.

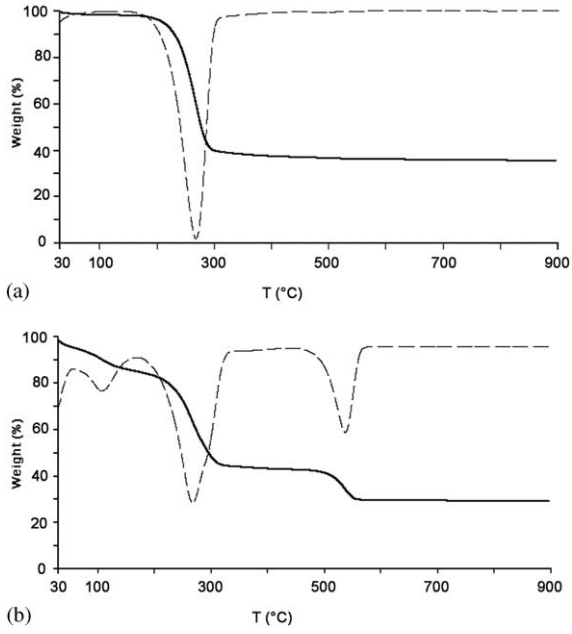

Fig. 1. TG-DTG plot of (a) the W-167-37, and of (b) the A-255-37 gels.

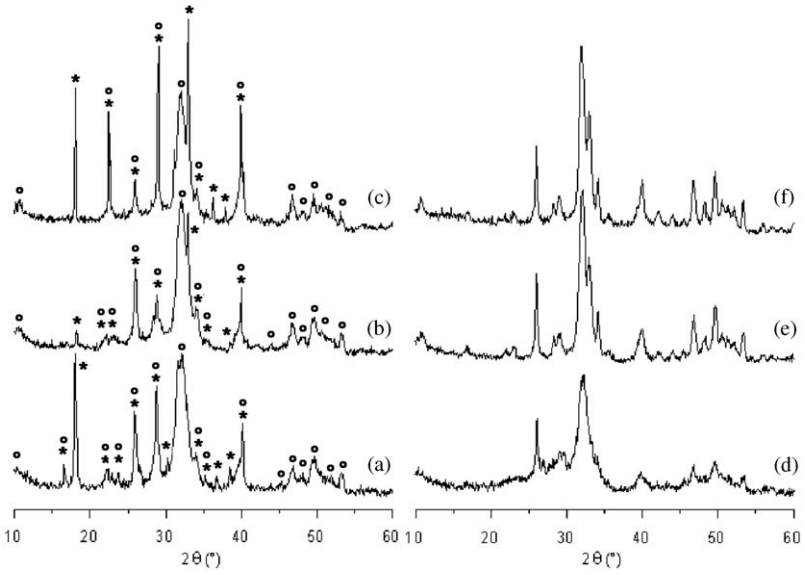

Fig. 2. Powder X-ray diffraction patterns of the gels obtained from sols at different Ca/P molar ratios: (a) W-100-80; (b) W-167-80; (c) W-255-80. (○) indicates the main peak of hydroxyapatite; (∗) indicates the main peaks of ammonium nitrate. The patterns of the same gels after heat treatment at 300°C are reported in (d), (e), and (f).

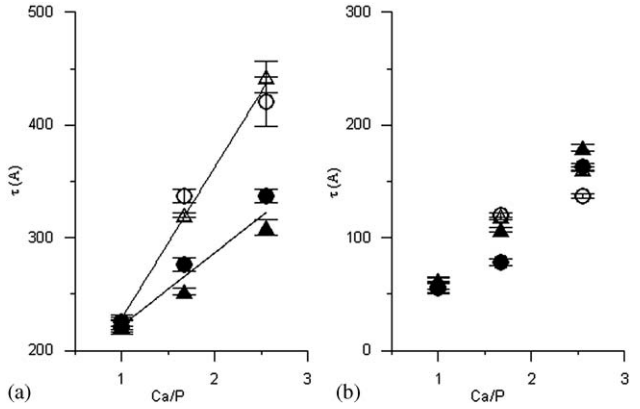

Fig. 3. Plot of the coherence lengths (τ_{hkl}) of the 0 0 2 (a) and 3 1 0 (b) reflections of HA obtained from the different gels after heat treatment at 300°C, as a function of the Ca/P molar ratio of the sols. (△): A-80; (○): A-37; (▲): W-80; (●): W-37.

Table 2
Crystalline phases present in the powder X-ray diffraction patterns of the gels submitted to heat treatment at different temperatures

Sample	300°C	500°C	700°C
A-100-37	HA	Ca Py	Ca Py
A-100-80	HA	Ca Py	Ca Py
W-100-37	HA	Ca Py	Ca Py
W-100-80	HA	Ca Py	Ca Py
A-167-37	HA	HA	HA
A-167-80	HA	HA	HA
W-167-37	HA	HA	HA
W-167-80	HA	HA	HA
A-255-37	HA	HA/CaC/Ca Py	HA/Ca Py/CaC
A-255-80	HA	HA/CaC/Ca Py	HA/Ca Py/CaC
W-255-37	HA	HA/CaC/Ca Py	HA/Ca Py/CaC
W-255-80	HA	HA/CaC/Ca Py	HA/Ca Py/CaC

Ca Py = calcium pyrophosphate; CaC = calcium carbonate (calcite).

Heat treatment at temperatures higher of 300°C provokes the formation of secondary phases in most of the gels. The phases present in the powder X-ray diffraction patterns of the gels submitted to heat treatment at different temperatures are reported in Table 2. The data indicate that the method utilized in this work yields HA as unique crystalline phase after heat treatment at 300°C, whatever the Ca/P molar ratio, the drying temperature and the precipitation medium. Furthermore, the products obtained with the stoichiometric Ca/P molar ratio of 1.67 are thermically stable, and do not transform into any other phase up to 700°C. At variance, heat treatment at 500°C is sufficient to provoke phase transition in the non-stoichiometric gels. The transition yields calcium pyrophosphate in the case

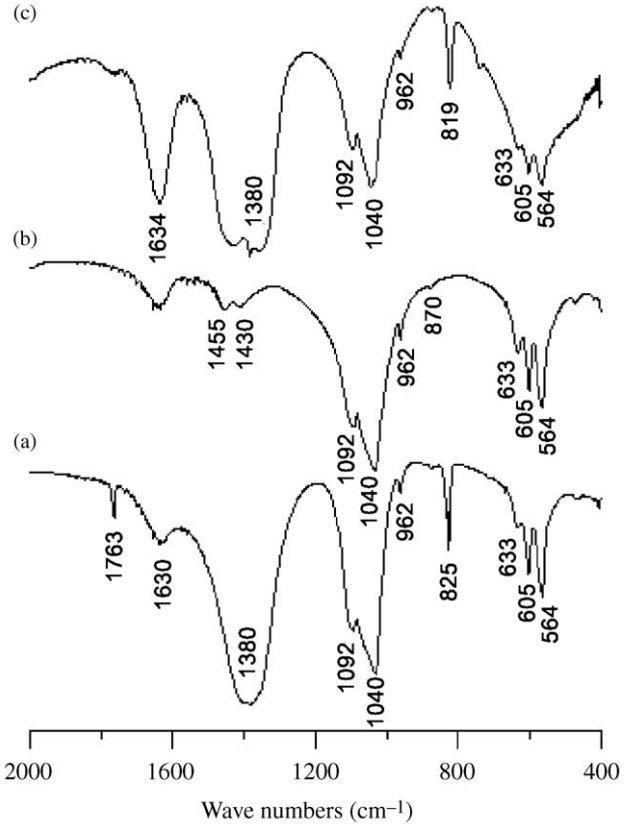

Fig. 4. Infrared absorption spectra: (a) W-167-37; (b) W-167-37 after heat treatment at 300°C; (c) W-255-37 after heat treatment at 300°C.

of the gels prepared with a Ca/P of 1.0, whereas calcium carbonate (calcite) and calcium pyrophosphate are obtained from the gels with a Ca/P of 2.55.

In agreement with the results of thermogravimetric and X-ray diffraction analyses, the FTIR spectra of the dried gels show the absorption bands characteristic of hydroxyapatite, together with two broad bands centered at about 1380 and 1630 cm^{-1}, and two bands at 825 and 1763 cm^{-1}, characteristic of nitrate (Fig. 4a). The relative intensity of the bands due to nitrate increases with the increase of the Ca/P molar ratio of the gels. The analysis of the FTIR spectra of 1.00- and 1.67-gels after heat-treatment at 300°C, indicate the absence of nitrate, an increase of the degree of crystallinity of the apatitic phase, and the presence of a small amount of carbonate. As a matter of fact, the spectrum of the W-167-37 gel heat treated at 300°C reported in Fig. 4b shows just the absorption bands of hydroxyapatite, which appear sharper than those in the spectrum reported in Fig. 4a, together with the bands at 1455–1430 and 870 cm^{-1}, associated with the carbonate symmetric and out of plane stretching mode, respectively. At variance, the IR spectra of the 2.55 gels after heat treatment at 300°C exhibit not only the absorption bands characteristic of

HA, but also quite intense absorption bands at about 819, 1380 and 1634 cm^{-1} (Fig. 4c). Since no evidence of nitrate was appreciated in the X-ray patterns of these samples it must be supposed that the IR bands are attributable to amorphous nitrate, or to its decomposition products, in agreement with the TG data.

Thus, the results of X-ray diffraction analysis indicate that the crystallization of hydroxyapatite occurs at 300°C, which is significantly lower than the temperatures generally reported in the literature [8,10,18–20], although recent results obtained using solution precursors with a Ca/P of 1 and an ethanol based sol–gel technique [20] report the presence of HA as the only crystalline phase at temperatures as low as 85°C. However, it must be pointed out that the absence of further crystalline phases in the X-ray patterns is not sufficient to state the absence of secondary compounds. As a matter of fact, although the X-ray diffraction patterns of the 2.55 gels heat treated at 300°C show the presence of HA as unique crystalline phase, the relative TG and IR data indicate that the products do not contain only hydroxyapatite. It must be concluded that it is not possible to obtain pure HA by heat treatment of gels with a Ca/P molar ratio largely exceeding the stoichiometric value. At variance, both the 1.67 and 1.00 gels after heat treatment at 300°C contain just hydroxyapatite. Furthermore, the stoichiometric gels are thermically stable and do not give any phase transition up to 700°C.

At the SEM investigation the surface of the dried gels appears constituted of HA crystals embedded in the gels, whereas HA flakes and crystallites can be appreciated in the porous fractured surface of the gels, as shown in the micrographs reported in Figs. 5a and b. After heat treatment at 300°C the structure becomes quite compact and homogeneous (Fig. 5c), suggesting that this process could be utilized to obtain compact thin films of HA.

3.2. Powders characterization

The powder X-ray diffraction patterns of the products obtained after filtration of the sols are reported in Fig. 6. The reflections are in agreement with the presence of a poor crystalline hydroxyapatite. The broadening of the reflections increases with the increase of the Ca/P molar ratio of the sols. Accordingly, the $\tau_{h\,k\,l}$ mean values, calculated using the line broadening of the 0 0 2 and 3 1 0 reflections, decrease as the Ca/P ratio of the sols increases from 1.00 to 2.55, indicating a decrease of the coherence length of the perfect crystalline domains. The $\tau_{h\,k\,l}$ values, and the Ca/P molar ratios of the solid phases, reported in Table 3 are the average values of those obtained for the samples prepared in water and those obtained from ethanol/water solution, since no significant variation was appreciated as a function of the precipitation medium. The decrease of crystallinity with

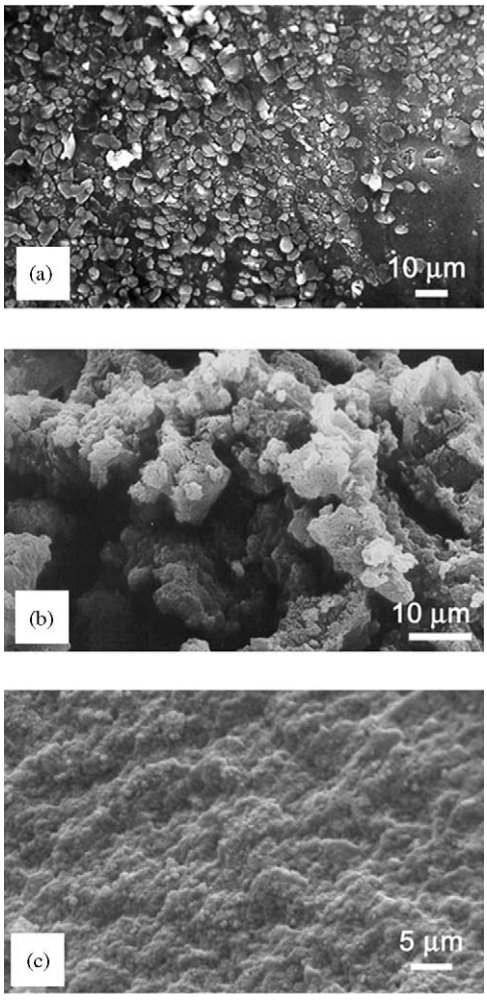

Fig. 5. SEM micrographs of the A-167-37 dried gel. (a) Surface of the gel; (b) fractured surface of the gel; (c) surface of the gel heat treated at 300°C.

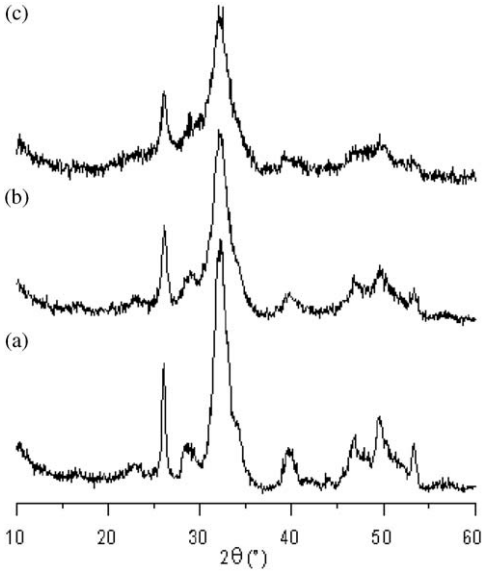

Fig. 6. Powder X-ray diffraction patterns of the powders obtained by filtering the sols prepared in aqueous medium at different Ca/P molar ratios: (a) 1.00; (b) 1.67; (c) 2.55.

Table 3
Coherence lengths (τ_{hkl}) of the perfect crystalline domains and Ca/P values of the powders obtained at different Ca/P molar ratio in solution

Ca/P in solution	τ_{002} (Å)	τ_{310} (Å)	Ca/P in the solid product
1.00	175 (1)	66 (2)	1.67
1.67	128 (2)	45 (2)	1.62
2.55	121 (3)	42 (4)	1.60

increasing the Ca/P of the sols is opposite to that found for the gels (Fig. 3). The increase of water content on increasing Ca/P molar ratio of the sols, due to the use of $Ca(NO_3)_2 \cdot 4H_2O$, might be responsible of a slower crystallization and a consequent increase of crystallinity of the gels. At variance, the simultaneous decrease of the crystallinity of the filtered products could be ascribed to the increase of the degree of supersaturation of the sols on increasing their Ca/P molar ratio, which might induce the precipitation of an increasing amount of amorphous calcium phosphate. The variation of the coherence lengths of the perfect crystalline domains of the filtered powders is in agreement with the results reported for samples prepared in similar conditions by Rodrigues and Lebugle [16]. These Authors observed a significant reduction of the τ_{002} and τ_{310} values when the samples are obtained from a sol with a Ca/P molar ratio of 1.6, in alcoholic medium, with respect to those obtained from a sol with a Ca/P molar ratio of 1.0 in aqueous medium. Our data clearly indicate that the presence of ethanol in the precipitation medium does not appreciably affect the structural properties of the filtered powders, whereas a major role is played by the Ca/P molar ratio of the sols. In agreement with the decrease of the crystallinity, the Ca/P molar ratios of the filtered powders decrease on increasing the Ca/P values in solution. Heat treatment of the samples at increasing temperatures does not provoke significant modification of the crystallinity of the apatitic phase, up to 700°C, when α- and β-TCP appear as secondary phases in the X-ray patterns of all the powder products. The relative amount of secondary phases increases as the Ca/P molar ratio of the sols increases, in agreement with the lower thermal stability of the less crystalline samples. The results of the TEM investigation indicate that also the morphology of the powders is strongly related to the Ca/P molar ratio of the sols. The TEM micrograph reported in Fig. 7a shows that the powders obtained from the 1.00-sols are constituted of very small thin crystals, which are about 20–40 nm long, and less than 10 nm wide. At variance, the TEM images of the powders filtered from the 1.67 sols show mainly the presence of small almost round particles (Fig. 7b), which fuse into bigger particles in the products of the 2.55 sols (Fig. 7c).

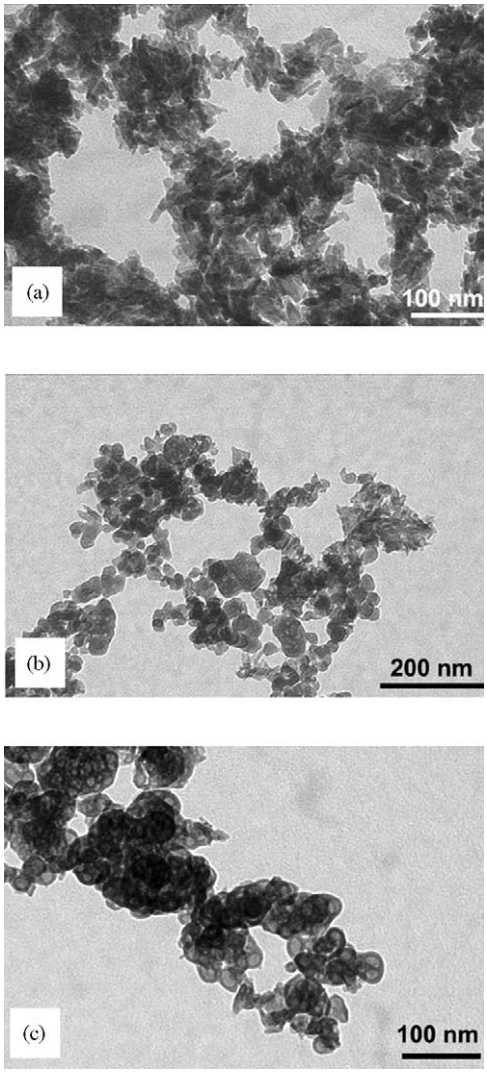

Fig. 7. TEM images of the powders obtained by filtering the sols prepared in aqueous medium at different Ca/P molar ratios: (a) 1.0; (b) 1.67; (c) 2.55.

4. Conclusions

The sol–gel process investigated in this study allows to synthesise HA at temperature as low as 300°C. The presence of ethanol in the reaction medium slightly affects the degree of crystallinity of HA, whereas variation in the value of the Ca/P molar ratio of the sols can be used to control the coherence length of the HA perfect crystalline domains, and the thermal stability of the gels. Filtration of the sols gives HA nanocrystals with morphology and structure closely related to the Ca/P molar ratio of the sol. Thus, the same approach could be successfully applied to the coating of substrates with compact HA thin films, as well as to the preparation of nanocrystalline HA powders.

Acknowledgments

This research was carried out with the financial support of MIUR, and the University of Bologna (Funds for Selected Research Topics).

References

[1] L.L. Hench, J. Wilson (Eds.), An Introduction to Bioceramics, World Scientific, Singapore, 1993.
[2] W. Suchanek, M. Yoshimura, J. Mater. Res. 13 (1998) 94–117.
[3] T. Kokubo, H.M. Kim, M. Kawashita, Biomaterials 24 (2003) 2161–2175.
[4] L.J. Jha, S.M. Best, J.C. Knoles, I. Rehman, J.D. Santos, W. Bonfield, J. Mater. Sci. Mater. Med. 8 (1997) 185–191.
[5] Y.C. Tsui, C. Doyle, T.W. Clyne, Biomaterials 19 (1998) 2015–2029.
[6] T.J. Webster, R.W. Siegel, R. Bizios, Biomaterials 21 (2000) 1803–1810.
[7] J.C. Elliott, Structure and Chemistry of the Apatites and Other Calcium Orthophosphates, Elsevier Science, The Netherlands, 1994.
[8] D.M. Liu, T. Troczynski, W.J. Tseng, Biomaterials 22 (2001) 1721–1730.
[9] A. Montenero, G. Gnappi, F. Ferrari, M. Cesari, E. Salvioli, L. Mattogno, S. Kaciulis, M. Fini, J. Mater. Sci. Mater. Med. 35 (2000) 2791–2797.
[10] C.S. Chai, K.A. Gross, B. Ben-Nissan, Biomaterials 19 (1998) 2291–2296.
[11] D.M. Liu, Q. Yang, T. Troczynski, W.J. Tseng, Biomaterials 23 (2002) 1679–1687.
[12] D.M. Liu, T. Troczynski, W.J. Tseng, Biomaterials 23 (2002) 1227–1236.
[13] M. Ashok, N.M. Sundaram, S.N. Kalkura, Mater. Lett. 57 (2003) 2066–2070.
[14] M.F. Hsieh, L.H. Perng, T.S. Chin, H.G. Perng, Biomaterials 22 (2001) 2601–2607.
[15] A. Rodrigues, A. Lebugle, Colloids Surf. A: Physiochem. Eng. Aspects 145 (1998) 191–204.
[16] H.P. Klug, L.E. Alexander, X-ray Diffraction Procedures for Polycrystalline and Amorphous Materials, Wiley-Interscience, New York, 1974.
[17] K.A. Gross, C.S. Chai, G.S.K. Kannangara, B. Ben-Nissan, L. Hanley, J. Mater. Sci. Mater. Med. 9 (1998) 839–843.
[18] P. Layrolle, A. Ito, T. Takishi, J. Am. Ceram. Soc. 81 (1998) 1421–1428.
[19] K.A. Gross, V. Gross, C.C. Berndt, J. Am. Ceram. Soc. 81 (1998) 106–112.
[20] T.A. Kuriakose, S.N. Kalkura, M. Palanichamy, D. Arivuoli, K. Dierks, G. Bocelli, C. Betzel, J. Cryst. Growth 263 (2004) 517–523.